CHAPTER FIVE

Modeling Mercury in Proteins ☆

J.M. Parks[*,†,1], **J.C. Smith**[*,†,1]
[*]Oak Ridge National Laboratory, Oak Ridge, TN, United States
[†]University of Tennessee, Knoxville, TN, United States
[1]Corresponding authors: e-mail address: parksjm@ornl.gov; smithjc@ornl.gov

Contents

Abstract

Mercury (Hg) is a naturally occurring element that is released into the biosphere both by natural processes and anthropogenic activities. Although its reduced, elemental form Hg(0) is relatively nontoxic, other forms such as Hg^{2+} and, in particular, its methylated form, methylmercury, are toxic, with deleterious effects on both ecosystems and humans. Microorganisms play important roles in the transformation of mercury in the environment. Inorganic Hg^{2+} can be methylated by certain bacteria and archaea

Methods in Enzymology, Volume 578
ISSN 0076-6879
http://dx.doi.org/10.1016/bs.mie.2016.05.041

to form methylmercury. Conversely, bacteria also demethylate methylmercury and reduce Hg^{2+} to relatively inert Hg(0). Transformations and toxicity occur as a result of mercury interacting with various proteins. Clearly, then, understanding the toxic effects of mercury and its cycling in the environment requires characterization of these interactions. Computational approaches are ideally suited to studies of mercury in proteins because they can provide a detailed molecular picture and circumvent issues associated with toxicity. Here, we describe computational methods for investigating and characterizing how mercury binds to proteins, how inter- and intraprotein transfer of mercury is orchestrated in biological systems, and how chemical reactions in proteins transform the metal. We describe quantum chemical analyses of aqueous Hg(II), which reveal critical factors that determine ligand-binding propensities. We then provide a perspective on how we used chemical reasoning to discover how microorganisms methylate mercury. We also highlight our combined computational and experimental studies of the proteins and enzymes of the *mer* operon, a suite of genes that confer mercury resistance in many bacteria. Lastly, we place work on mercury in proteins in the context of what is needed for a comprehensive multiscale model of environmental mercury cycling.

1. INTRODUCTION

1.1 Mercury Toxicity

It is well known that mercury (Hg) is toxic to living organisms. Hg^{2+} and the monomethylated form of Hg, methylmercury (CH_3HgR, where R is an anionic ligand), are particularly dangerous to living organisms. Their toxicity results from the ability to bind strongly to various biomolecules and disrupt their normal function. Methylmercury is also able to cross the blood–brain barrier and is therefore a neurotoxin. It is generally accepted that Hg has no known beneficial function in any living organism, although that view has been challenged recently (Gregoire & Poulain, 2016).

Proteins play important roles in the environmental processes that transform Hg from one form to another. They are also important contributors to Hg toxicity in humans. Notably, Hg^{2+} has an extremely high affinity for thiol(ate) groups, which are present in the amino acid cysteine in numerous proteins. Hg^{2+} can also outcompete other metals, such as Zn and Fe, in the binding sites of metalloproteins or metalloenzymes. Therefore, understanding how Hg interacts with proteins is of both fundamental and practical importance. Specific Hg–protein interactions play key roles in binding to specific functional groups, reduction/oxidation and methylation/demethylation.

1.2 Inorganic Hg Chemistry

Before beginning a discussion of the interaction of Hg with proteins, it is important to provide a brief summary of the aqueous-phase chemistry of inorganic Hg. The most relevant oxidation states are Hg^0 and Hg^{2+}, so we limit the present discussion to these two forms. Elemental Hg(0) is not particularly toxic, but is readily oxidized to highly reactive and highly toxic Hg^{2+}. Hg^{2+} does not generally exist as an isolated dication in aqueous solution. Rather, it is essentially always bound to two or more anionic or neutral ligands. Among the most strongly interacting ligands are thiolates (RS^-), as found in the amino acid cysteine and the cellular redox mediator glutathione. Other low molecular weight thiolates, such as hydrosulfide (HS^-), also bind Hg^{2+} with high affinity. Hg^{2+} typically binds two or three thiolates to form bis or tris species of the form $[Hg^{II}(SR)_n]^{2-n}$, $n=2$ or 3. Selenides, which are chemically similar to but generally less abundant than sulfides, also interact strongly with Hg^{2+}. In the absence of thiolates, Hg^{2+} binds other functional groups, such as hydroxides, halides, carboxylates, and amines, with affinities that span many orders of magnitude in terms of binding constants. In complex biological systems and natural environments, Hg encounters numerous chemical species. Although thermodynamic quantities (ie, solvation and ligand-binding free energies) have been measured for many Hg-containing molecules, there is still a fairly large degree of uncertainty in many of these values. It is therefore important to quantify Hg interactions in a consistent way so that Hg speciation in complex systems can be understood at a fundamental level.

1.3 Quantum Chemistry

Quantum chemistry is a natural means of determining the driving forces behind the speciation of Hg^{2+}. Density functional theory (DFT) is the standard method of choice for quantum chemistry because it can provide accurate structures and energies provided that a suitable density functional and basis set are used. However, wave function methods, such as MP2, can provide similar or better accuracy than DFT. It is also critical to describe relativistic effects adequately in Hg-containing systems. We have found that small-core, quasi-relativistic effective core potentials (ECPs) perform quite well in this regard.

Because our emphasis is on aqueous speciation and reactivity, it is particularly important to account properly for the effects of solvation. It is common to carry out quantum chemical calculations in combination with a

polarizable continuum model (PCM) representation of the solvent. However, continuum approaches are known to be unable to describe strong, short-range, anisotropic interactions with the solvent. A well-known example of the limitations of continuum solvation is the inability to describe explicit hydrogen bonding between the solute and solvent, but other types of direct interactions such as Hg–O coordination can also play important roles. Thus, it is becoming increasingly more common to include a relatively small number ($n = 1–18$) explicit water molecules as part of the supersolute to describe short-range solute–solvent interactions and implicit (ie, PCM) solvation to describe long-range, bulk solvation effects. Such an approach is often referred to as a mixed discrete-continuum method.

1.4 Hydration Free Energies

In a recent study, we used dispersion-corrected DFT and MP2 calculations in combination with a mixed discrete-continuum solvation approach to compute hydration free energies for the group 12 divalent metal cations Zn^{2+}, Cd^{2+}, and Hg^{2+} and the anions SH^-, OH^-, Cl^-, and F^- (Riccardi, Guo, Parks, Gu, Liang, et al., 2013; Riccardi, Guo, Parks, Gu, Summers, et al., 2013). Long-range solvation effects were described by the SMD solvent model (Marenich, Cramer, & Truhlar, 2009). As is commonly done, we used thermodynamic cycles to compute the hydration free energies, $\Delta G_{aq}{}^*$. In such an approach, (super)solute geometries are optimized in the gas phase, and then solvation energies for each reactant and product are computed as the difference in energy between the gas-phase and PCM-solvated molecules. Including explicit solvent molecules complicates the matter by introducing additional degrees of freedom, and care must be taken to account properly for standard states. More thorough discussions of the challenges associated with mixed discrete-continuum solvation have been covered elsewhere (Bryantsev, Diallo, & Goddard, 2008; Riccardi, Guo, Parks, Gu, Liang, et al., 2013; Riccardi, Guo, Parks, Gu, Summers, et al., 2013).

We considered various schemes for selecting the optimal number of explicit water molecules to include along with the solute, and we found that the use of a constant number for a given ion type (ie, metal cation or inorganic ion) provided the greatest accuracy. For the metal cations and anions, inclusion of 10 and 8 explicit water molecules, respectively, was found to provide the lowest errors compared to experimentally measured relative hydration free energies. Although hybrid DFT performed quite well in this

context, the best agreement with experiment came from MP2, which yielded a standard deviation of 2.3 kcal/mol. In another recent DFT study (Afaneh, Schreckenbach, & Wang, 2014), the use of four or five explicit water molecules to saturate the first solvation shell of the solutes was recommended in the context of mixed discrete-continuum calculations. Similar accuracy to our approach was obtained.

1.5 Hg–Ligand Binding Free Energies

Based on the accuracy obtained for the computed (relative) hydration free energies, we extended the approach to Hg–ligand binding free energies (Riccardi, Guo, Parks, Gu, Summers, et al., 2013). In that work, we considered three hydrochalcogenide ligands (OH^-, SH^-, and SeH^-) and three halide ligands (F^-, Cl^-, and Br^-). Binding of these ligands to Hg^{2+} proceeds as follows:

$$Hg^{2+} + L_1 + L_2 \leftrightharpoons HgL_1L_2.$$

Using the dispersion-corrected (Grimme, Antony, Ehrlich, & Krieg, 2010; Grimme, Ehrlich, & Goerigk, 2011) B3PW91 hybrid density functional (Becke, 1993; Perdew & Wang, 1992) (ie, B3PW91-D3), along with small-core ECPs (Peterson & Puzzarini, 2005) and the SMD solvent model (Marenich et al., 2009), aqueous relative binding free energies ($\Delta\Delta G_{aq}$*) were computed and compared with experimental values. Here, we found that it was sufficient to include only two explicit water molecules for each species to obtain highly accurate results (see later). In this case, we obtained a mean signed error of 0.7 kcal/mol and a standard deviation of 0.8 kcal/mol (Fig. 1). The calculations reproduced the correct trend, $Hg(SH)_2 > Hg(OH)_2 > HgBr_2 \simeq Hg(OH)Cl > HgCl_2$, in the experimentally determined aqueous binding affinities.

With quantum chemistry it is also possible to dissect individual energetic contributions to gain insight into the underlying physical phenomena that govern ligand-binding behavior. Solvation effects can be addressed by comparing processes in the gas and aqueous phases with varying descriptions of the solvent. In this case, that approach led to somewhat surprising results. We examined the behavior of the computed binding free energies in four stages. First, we considered only gas-phase species. We then added one explicit water molecule, then two explicit water molecules, and finally two explicit water molecules plus continuum solvation (Fig. 2).

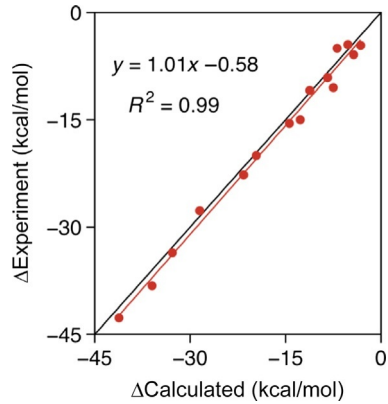

Fig. 1 Experimental and theoretical binding free energy differences for a set of neutral HgR_2 complexes. *Adapted with permission from Riccardi, D., Guo, H.-B., Parks, J. M., Gu, B., Summers, A. O., Miller, S. M., … Smith, J. C. (2013). Why mercury prefers soft ligands.* Journal of Physical Chemistry Letters, 4, *2317–2322. doi:10.1021/jz401075b. Copyright 2013 American Chemical Society.*

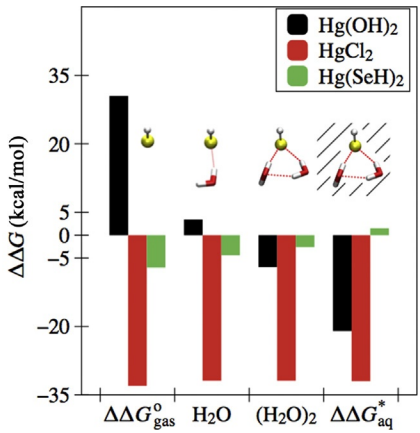

Fig. 2 Differences in binding free energy relative to $Hg(SH)_2$ with varying descriptions of the solvent. *Left* to *right*: gas phase, one and two explicit water molecules, and two explicit water molecules with SMD continuum solvation. The optimized geometries for SH^-, $H_2O{\cdot}SH^-$, and $(H_2O)_2{\cdot}SH^-$ are also shown. The *shaded region* denotes continuum solvation. *Reprinted with permission from Riccardi, D., Guo, H.-B., Parks, J. M., Gu, B., Summers, A. O., Miller, S. M., … Smith, J. C. (2013). Why mercury prefers soft ligands.* Journal of Physical Chemistry Letters, 4, *2317–2322. doi:10.1021/jz401075b. Copyright 2013 American Chemical Society.*

In aqueous solution, formation of $Hg(SH)_2$ is 22.8 kcal/mol more favorable than $Hg(OH)_2$, and our calculations reproduce this free energy difference. On the other hand, in the gas phase the formation of $Hg(SH)_2$ from its constituent ions in the gas phase is ~30 kcal/mol *less* favorable than $Hg(OH)_2$. Inclusion of a single water molecule makes the binding free energies nearly equal, and the formation of $Hg(SH)_2$ becomes more favorable than $Hg(OH)_2$ when only two water molecules are included. When two water molecules and continuum solvation are included, the experimental binding free energy difference between the two complexes is reproduced almost exactly (Fig. 2). Thus, solvation effects are responsible for a 52 kcal/mol change in the relative binding free energies between these two molecules upon transferring them from the gas phase to aqueous solution, and the majority of this effect is imparted by water molecules that interact strongly with the solutes.

2. MICROBIAL INTERACTIONS WITH HG

We now turn to modeling mercury in proteins. Microorganisms are key players in the global cycling of Hg. Various bacteria and archaea are involved in Hg toxification, detoxification, or both. Whereas some microbes methylate Hg, others demethylate it. Some can both methylate and demethylate it. Here, we provide a synopsis of some of the important proteins and enzymes that mediate the transformation of Hg species. We then discuss the computational approaches we have used to provide mechanistic insight into these processes.

2.1 Bacterial Hg Resistance

Many aerobic bacteria are able to thrive in Hg-contaminated environments because they possess the Hg resistance, or *mer*, operon. The prototypical, broad-spectrum *mer* operon encodes several proteins and enzymes. In addition to a transcriptional regulator, MerR, Hg-resistant bacteria produce various membrane-bound transporter proteins (MerC, MerT, and others), a periplasmic metallochaperone (MerP), and two key enzymes (MerB and MerA). Our studies have focused specifically on the two enzymes MerB and MerA, and the transcriptional regulator, MerR.

A common theme in the *mer* proteins is the ubiquity of pairs of Cys residues that bind Hg^{2+} and orchestrate its transfer throughout the cell until it is ultimately reduced to Hg^0 and no longer poses a threat to the cellular machinery.

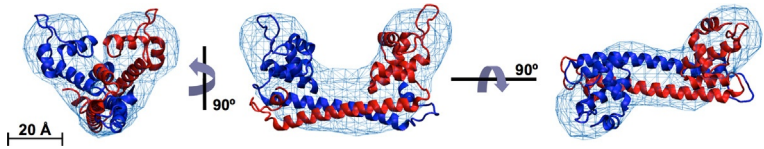

Fig. 3 Best-fitting conformation of Hg(II)-MerR obtained from MD simulations superimposed onto the three-dimensional molecular envelope (*blue mesh*) as determined by SAXS. *Reprinted from Guo, H.-B., Johs, A., Parks, J. M., Olliff, L., Miller, S. M., Summers, A. O., … Smith, J. C. (2010). Structure and comformational dynamics of the metalloregulator MerR upon binding of Hg(II).* Journal of Molecular Biology, 398, *555–568. doi: 10.1016/j.jmb.2010.03.020. Copyright 2010, with permission from Elsevier.*

2.2 MerR

The bacterial metalloregulator MerR controls transcription of the *mer* operon in Hg-resistant bacteria. Although related proteins had been characterized by X-ray crystallography, MerR had proven difficult to crystallize. Using small-angle X-ray scattering (SAXS) and molecular dynamics (MD) simulation on a homology of the protein, we sought to determine its structure and conformational dynamics in solution to gain insight into possible mechanisms of transcriptional control (Fig. 3). From the MD simulations, interdomain motions on the ~10 ns time scale were found for the two DNA-binding domains of the homodimeric protein. Thus, Hg^{2+}-bound MerR exhibits conformational dynamics that induce conformational changes in the *mer* operator DNA such that transcription is initiated by RNA polymerase. Recent work performed elsewhere confirmed that the structures obtained with SAXS and MD are in good agreement with X-ray crystal structures of Hg(II)-bound MerR (Chang, Lin, Zou, Huang, & Chan, 2015).

2.3 MerB

The organomercurial lyase, MerB, cleaves Hg–C bonds in organomercurials according to the following reaction:

$$\left[\mathrm{R-Hg^{II}}\right]^{+} \rightarrow \mathrm{Hg^{2+}} + \mathrm{R-H},$$

where R is an alkyl or aryl substituent, with the most prevalent organomercurial species being methylmercury. X-ray crystal structures of Hg-free and Hg^{2+}-bound MerB have been solved (Lafrance-Vanasse, Lefebvre, Di Lello, Sygusch, & Omichinski, 2009), and the active site contains two Cys and one Asp residue (Fig. 4). All three of these residues are required for activity (Parks et al., 2009; Pitts & Summers, 2002).

A common method for simulating enzyme catalysis is the quantum mechanical/molecular mechanical (QM/MM) approach (Senn & Thiel,

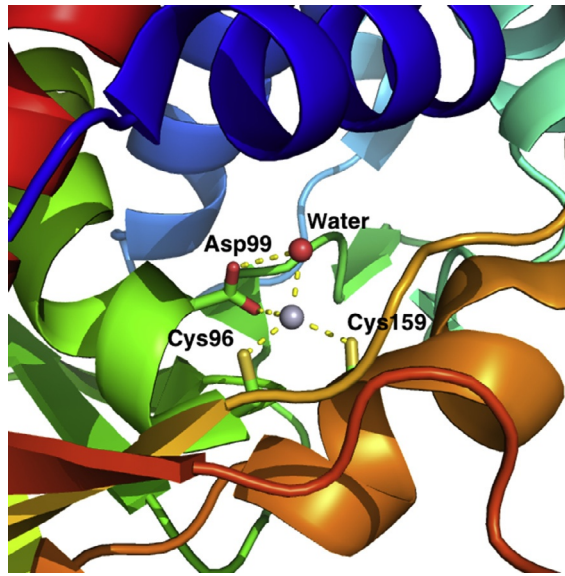

Fig. 4 Active site of Hg^{2+}-bound MerB (PDB entry 3F2F (Lafrance-Vanasse et al., 2009)). *Adapted with permission from Parks, J. M., Guo, H., Momany, C., Liang, L. Y., Miller, S. M., Summers, A. O., & Smith, J. C. (2009). Mechanism of Hg–C protonolysis in the organomercurial lyase MerB.* Journal of the American Chemical Society, 131*(37), 13278–13285. doi:10.1021/Ja9016123. Copyright 2009 American Chemical Society.*

2009; Warshel & Levitt, 1976). Alternatively, QM-only cluster models (Siegbahn & Himo, 2011) have been used successfully for numerous enzymes, particularly transition metal-containing metalloenzymes. MerB is not a metalloenzyme in the sense that it uses a metal cofactor (because methylmercury is instead the substrate), and Hg is not a transition metal. However, we recognized that there are certain parallels between MerB and metalloenzymes. In such a case, coordination chemistry tends to be the most important aspect to consider. Thus, we used a quantum chemical cluster approach to study Hg–C cleavage in MerB (Parks et al., 2009).

To construct the active-site model, the Cartesian coordinates of the side chains of Cys96, Asp99, and Cys159 (*Escherichia coli* numbering) along with Hg^{2+} and a single crystallographic water molecule were extracted from the X-ray crystal structure of Hg^{2+}-bound MerB. Missing hydrogens were added and the model was manually modified to include a $[CH_3Hg]^+$ substrate rather than the Hg^{2+} product. We performed hybrid DFT optimizations with the B3PW91 density functional (Becke, 1993; Perdew & Yue, 1986), a suitable ECP for Hg (Andrae, Haussermann, Dolg, Stoll, & Preuss, 1990), and a polarizable continuum representation to describe the

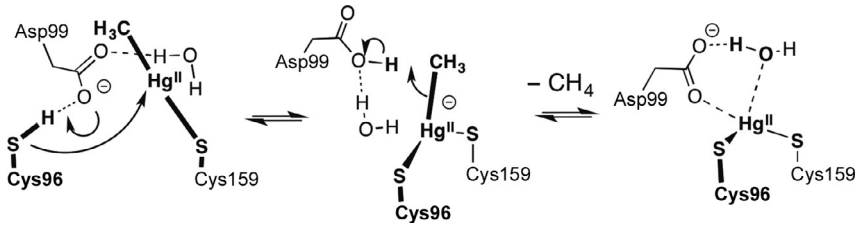

Fig. 5 Proposed mechanism of MerB as deduced from quantum chemical cluster calculations with polarizable continuum solvation.

protein/solvent environment around the active site. As is common in similar studies, a dielectric constant of 4 was used to describe the mostly hydrophobic active site. Optimized geometries of various reactant, intermediate, transition state, and products were then used to map out the energetic landscape of the reaction and identify energetically favorable reaction mechanisms.

These simple QM cluster models were able to reproduce the experimentally observed trend in enzymatic turnover (ie, k_{cat}) for the three organomercurial substrates considered. Furthermore, the computed activation free energies were all within about 1 kcal/mol of the experimental values derived from k_{cat} using transition state theory. From the calculations, the most energetically favorable reaction mechanism emerged (Fig. 5), which we summarize here. Initially, CH_3Hg^+ is coordinated to only one of the active-site Cys residues and the other Cys remains a neutral thiol. The second Cys residue then coordinates to methylmercury to form a trigonal species, and transfers its proton to Asp99. Coordination by two Cys residues weakens the Hg–C bond substantially, and the Asp is ideally positioned to donate its proton to the leaving group carbon. The result is a protonolytic cleavage of the Hg–C bond, with Hg^{2+} remaining bound in the active site as observed crystallographically. Thus, MerB accomplishes the demethylation of methylmercury by quenching an otherwise highly reactive carbanion through protonation as it begins to form. The calculations showed that coordination of the methylmercury substrate by two Cys thiolates is sufficient to activate the Hg–C bond, redistributing electron density into the methyl leaving group and away from the proton on the catalytic acid, Asp99.

2.4 MerA

After methylmercury has been demethylated by MerB to form Hg^{2+}, it is reduced by the mercuric reductase, MerA, an NADP-dependent

flavoenzyme. Although numerous MerA variants exist, our studies have focused on those variants that consist of a homodimeric catalytic core domain with each monomer bearing an N-terminal metallochaperone-like domain, NmerA, connected to the catalytic core domain by a flexible and disordered peptide linker ~30 residues in length. This form of MerA contains multiple pairs of Cys residues that sequentially bind Hg^{2+} and orchestrate its handoff to the next pair.

Initially, Hg^{2+} is bound to NmerA through two highly conserved Cys residues. Because NmerA is linked to the core domain, the two subunits remain in relatively close proximity to the core. In one study (Johs et al., 2011), we used a combination of SAXS and small-angle neutron scattering along with MD simulation to characterize the flexibility of full-length MerA. Using a simple rigid-body MD approach, we generated a large number of linker conformations of the NmerA domains relative to the core. We then computed X-ray scattering profiles and compared them with the experimentally determined profile. The best fits to the experimental data were obtained when a small ensemble of disordered linker conformations was used, suggesting that the NmerA domains and linkers are highly flexible and sample large regions of conformational space.

The dynamic nature of the NmerA metallochaperone domains may facilitate the efficient capture and subsequent transfer of Hg^{2+} to the core domain for subsequent reduction. In a novel approach to protein–protein docking (Johs et al., 2011), we also used SAXS/SANS and MD to reveal how NmerA docks to the core domain to accomplish the interdomain transfer of Hg^{2+}. Scattering profiles were obtained for a variant of the enzyme with a disulfide linkage connecting one Cys on NmerA to another Cys at the C-terminus of the core domain. Computational models of the system in various interdomain orientations were generated and subjected to MD simulation. As for the previous models, scattering profiles were computed for each model and compared with the experimental data. In this case, a single MD conformation was sufficient to match the experimental scattering profile, which revealed the most likely docking configuration between the two domains (Fig. 6).

In subsequent work, neutron spin-echo (NSE) spectroscopy was combined with all-atom, explicitly solvated and coarse-grained MD simulation of MerA (Hong et al., 2014) (Fig. 7). NSE permits large-scale motions of proteins to be probed directly. In both the experiments and the simulations, the NmerA domains were found to interact with the core domain primarily through electrostatic interactions. The observed compact but dynamic

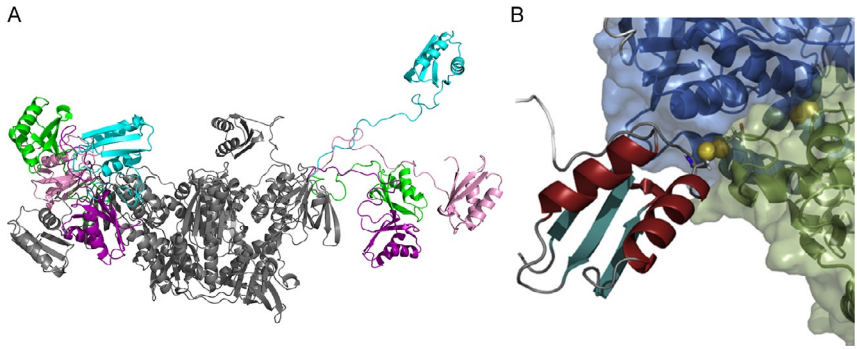

Fig. 6 (A) Representative ensemble of conformations obtained from rigid-body MD simulation. Including multiple conformations improve the agreement with experimental SAXS data compared to using only a single, best-fitting conformation. (B) Docking orientation of NmerA to the catalytic core of MerA as determined from small-angle scattering and MD simulation. *Reprinted from Johs, A., Harwood, I. M., Parks, J. M., Nauss, R. E., Smith, J. C., Liang, L. Y., & Miller, S. M. (2011). Structural characterization of intramolecular Hg^{2+} transfer between flexibly linked domains of mercuric ion reductase.* Journal of Molecular Biology, 413*(3), 639–656. doi:10.1016/J.Jmb.2011.08.042. Copyright 2011, with permission from Elsevier.*

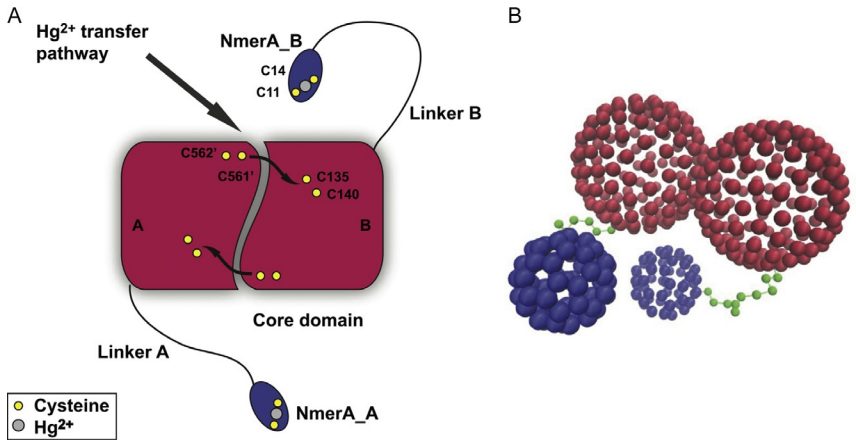

Fig. 7 (A) Schematic illustration of the MerA homodimer and scheme for intramolecular Hg^{2+} transfer. Hg^{2+} is first bound by the NmerA cysteines (C11 and C14), and is then delivered to the C-terminal cysteines of the other monomer (C561′ and C562′). Lastly, Hg^{2+} is transferred to a pair of cysteines in the catalytic site of the core (C135 and C140) where it is then reduced to Hg^0. (B) Simplified coarse-grained model for MerA with a rigid two-sphere core (*red*) and small spheres for the NmerA domains (*blue*), which are connected to the core by flexible linkers (*green*). *Reprinted from Hong, L., Sharp, M. A., Poblete, S., Biehl, R., Zamponi, M., Szekely, N., … Smith, J. C. (2014). Structure and dynamics of a compact state of a multi-domain protein, the mercuric ion reductase.* Biophysical Journal, 107, *2014, 393–400. doi: 10.1016/j.bpj.2014.06.013. Copyright 2014, from Elsevier.*

arrangement of the domains may facilitate transfer of Hg^{2+} from NmerA to the core, where it is then reduced to Hg^0.

2.5 Intramolecular Hg^{2+} Transfer

Having established the role of conformational dynamics in MerA, we now discuss the chemistry of Hg^{2+} transfer in MerA. Binding of Hg^{2+} by two Cys thiolates is thermodynamically extremely favorable. Hg^{2+} and $[RHg(II)]^+$ species have extremely high affinities for thiols, with K_{form} values for Hg bis thiolate complexes on the order of $\sim 10^{35}$–10^{40} M^{-2} (Stricks & Kolthoff, 1953). However, these complexes can undergo rapid exchange between thiols (Cheesman, Arnold, & Rabenstein, 1988). That is, one of the thiolates can readily dissociate, provided that a third thiolate first coordinates to Hg. Thus, a transient, trigonal $[Hg^{II}(Cys)_3]^-$ species is expected to be important in Hg^{2+} transfer reactions. Also, acid–base chemistry in which thiols are deprotonated to generate nucleophilic thiolates, or coordinated thiolates are protonated to generate neutral leaving groups, can enhance the rates of Hg^{2+} transfer among pairs of thiols. QM/MM calculations were used to identify a possible mechanism for the intramolecular Hg^{2+} transfer in MerA (Lian et al., 2014), which can be considered a prototype for Hg transfer in other *mer* protein and enzymes. Specifically, an X-ray crystal structure of the catalytic core of MerA with Hg^{2+} bound to the C-terminal Cys pair was used as a starting point for simulating Hg^{2+} transfer from the surface of the protein to the buried, inner pair of Cys residues in the active site (Lian et al., 2014).

From the computed Hg^{2+} transfer pathway (Lian et al., 2014), we note that Hg^{2+} is always paired with two or more thiolates. In both the initial (Hg bound to Cys558′ and Cys 559′) and final (Hg bound to Cys136 and Cys141) states (Fig. 8), the $Hg(Cys)_2$ complexes bear a neutral charge. As Hg^{2+} is transferred from the solvent-exposed protein surface to the buried catalytic site, a proton is transferred in the opposite direction. Thus, a net negative charge is transferred over ~8 Å. The key mechanistic insight from the simulations is that Hg^{2+} transfer is facilitated by coupling the competitive binding of pairs of Cys residues with the proton affinities of the thiolates. These principles are expected to be general to other proteins and enzymes of the *mer* operon and metal ion trafficking proteins in other biological systems.

Once Hg^{2+} is bound to the active-site Cys pair, NADPH transfers hydride to FAD to form $FADH^-$, which reduces the Cys–Hg(II)–Cys complex to produce Hg^0. Because it no longer has any appreciable affinity for Cys thiolates or other functional groups, Hg^0 simply diffuses out of the bacterial cell.

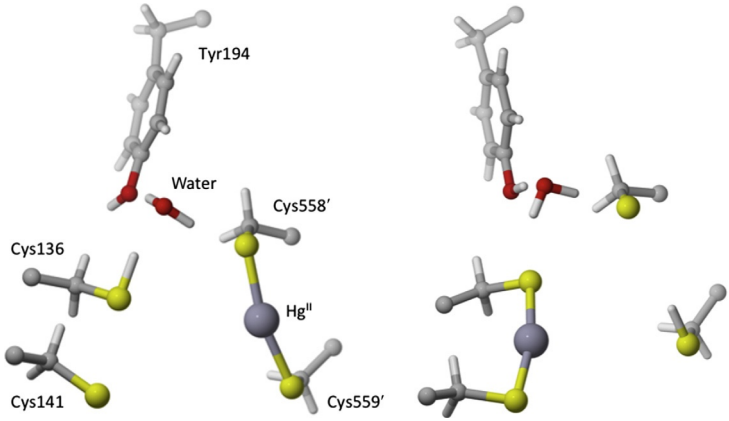

Fig. 8 Initial (*left*) and final (*right*) states from QM/MM simulations of the intramolecular transfer of Hg^{2+} from the C-terminal Cys pair on the surface of the protein to the Cys pair in the active site of MerA. Only the atoms in the QM subsystem are shown. *Adapted with permission from Lian, P., Guo, H. B., Riccardi, D., Dong, A. P., Parks, J. M., Xu, Q., … Guo, H. (2014). X-ray Structure of a Hg^{2+} complex of mercuric reductase (MerA) and quantum mechanical/molecular mechanical study of Hg^{2+} transfer between the C-terminal and buried catalytic site cysteine pairs.* Biochemistry, 53*(46), 7211–7222. doi:10.1021/bi500608u. Copyright 2014 American Chemical Society.*

2.6 Hg Methylation

In the late 1960s, it was shown that anaerobic microorganisms could produce methylmercury from inorganic Hg. However, the genetic and biochemical basis for the reaction remained elusive for more than four decades. In the early to mid-1990s, Hg methylation was shown to be an enzyme-catalyzed process (Choi, Chase, & Bartha, 1994a) involving a protein with a corrinoid, ie, vitamin B12-like, cofactor (Choi & Bartha, 1993). The methylation process was also shown to be associated with the reductive acetyl-CoA, or Wood–Ljungdahl (WL) pathway (Choi, Chase, & Bartha, 1994b), which is involved in acetogenesis in anaerobic bacteria (Ragsdale & Pierce, 2008). Numerous bacteria possess the WL pathway, but only a small number were known to be Hg methylators, and there was no obvious phylogenetic pattern to suggest which organisms could and could not perform the reaction. It was unclear which specific protein or proteins were required to methylate Hg.

To identify the genes and corresponding proteins responsible for Hg methylation, we approached the problem by considering the chemistry that would be required if a corrinoid protein were involved. There is only one corrinoid protein in the WL pathway, and this protein, called the corrinoid iron–sulfur protein (CFeSP), accepts and then transfers CH_3^+ in the

biosynthesis of acetyl-CoA. In CFeSP, there is no axial cobalt ligand *trans* to the methyl group, and this configuration is known to favor CH_3^+ transfer. The dominant form of Hg in cells is Hg^{2+} bound to two thiolates (Colombo, Ha, Reinfelder, Barkay, & Yee, 2013). It is not possible to form a Hg–C bond between Hg^{2+} and CH_3^+ because there are simply not enough electrons. A more plausible reaction leading to Hg–C bond formation would involve a methyl carbanion, CH_3^-, which can in principle be delivered by a methylated corrinoid. Such a protein must be different from CFeSP to perform the required chemistry (as CFeSP transfers CH_3^+), so we hypothesized that a corrinoid protein that could methylate Hg^{2+} would need to have an electron-donating group in the axial position opposite the methyl group. We hoped that this protein might be similar enough in sequence to the CFeSP that we could search for such a protein in sequence databases. Thus, we performed a BLAST search with the sequence of CFeSP against the translated genome of a known Hg-methylating organism. Although CFeSP is not present in this organism, a portion of a single protein sequence encoded in the entire genome was a match, and this sequence corresponded to the corrinoid-binding domain of CFeSP. We then found that this newly identified protein sequence is encoded in the genomes of all known Hg-methylating bacteria, but absent in all nonmethylators. X-ray crystal structures have been determined for CFeSP (Svetlitchnaia, Svetlitchnyi, Meyer, & Dobbek, 2006), so we generated a homology model of the corrinoid-binding domain. To our surprise, the model revealed a strictly conserved Cys residue positioned ideally for coordination to cobalt on the lower face of the cofactor in what we refer to as a "Cys-on" cobalt binding configuration (Fig. 9A). A Cys thiolate is expected to donate electron density into the cofactor, stabilizing the Co^{3+} oxidation state and facilitating transfer of CH_3^- to a Hg^{2+}-containing substrate molecule.

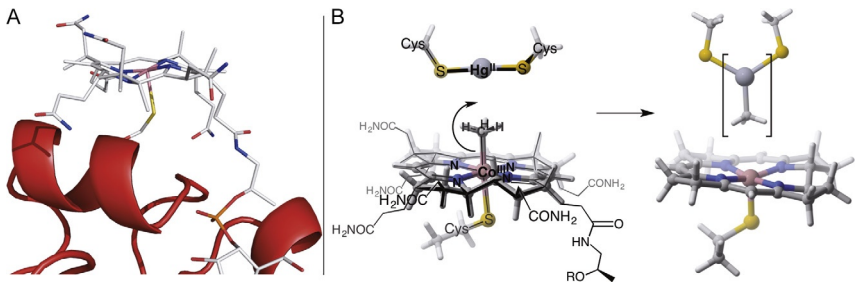

Fig. 9 (A) Predicted "Cys-on" binding of the corrinoid cofactor in a homology model of HgcA. (B) Quantum chemical model used to investigate methyl transfer from HgcA to a $Hg^{II}(Cys)_2$ substrate. The resulting methylmercury product is shown in *square brackets*.

Corrinoids are known to require low-potential electrons to achieve the reduction of Co to the Co^{1+} oxidation state. Intriguingly, a second gene encoding a ferredoxin is always present nearby in the genomes.

Up to this point, the genes and proteins proposed to be involved in Hg methylation had yet not been tested and verified experimentally. It is important to acknowledge the Herculean experimental effort performed by our experimental collaborators that was needed to confirm the predictions. No genetic system for deleting genes in any of the predicted Hg-methylating bacteria, so one had to be developed essentially from scratch. Fortunately, the predictions were ultimately confirmed (Parks et al., 2013), so it was worth the effort. When either gene was deleted, the bacteria no longer produced methylmercury. When the genes were reintroduced into the genome, methylation activity was restored. We now refer to the corrinoid protein as HgcA and the ferredoxin as HgcB, and the genes encoding these proteins have been found in the genomes of numerous bacteria and archaea.

In subsequent work, we used quantum chemical models of HgcA and computed reaction free energies for the transfer of a methyl group to a $Hg^{II}(SR)_2$ substrate (Fig. 9B) (Zhou, Riccardi, Beste, Smith, & Parks, 2014). We compared the favorability of transferring either a methyl radical or methyl carbanion, and found that carbanion transfer was more favorable when (continuum) solvation effects were included. Furthermore, we showed that the axial Cys ligand indeed promotes carbanion transfer compared to a His ligand, the latter of which is common in corrinoid proteins. Site-directed mutagenesis experiments provided further support for Co–Cys coordination in HgcA and its role in methylation. Replacement of Cys with Ala completely abolished Hg methylation activity in vivo (Smith et al., 2015).

2.7 Hg Uptake

Hg exists in numerous forms and in natural environments. Often, these molecules come into contact with microbial cells and interact with functional groups on cell surfaces leading to adsorption, ligand exchange, and redox transformation. Identifying the particular Hg-containing molecules that are bioavailable for cellular uptake into these cells is an active area of research, but $Hg^{II}(Cys)_2$ and related complexes are known to be assimilated readily by aerobic bacteria (Schaefer & Morel, 2009). It has been proposed that Hg is mistaken for other metals by membrane-bound transporters (Schaefer et al., 2011), but no specific transporters have yet been identified.

It is not known how Hg is transported throughout the cell once it has entered, but thiol-containing small molecules or proteins are expected to play important roles.

3. FUTURE PERSPECTIVES

Ten years ago the application of computational chemistry to studies of Hg interacting with proteins was practically nonexistent. Now, however, many of the tools are in place to derive a comprehensive description of Hg cycling not only in proteins but also in the natural environment.

Predictive understanding of environmental Hg cycling is lacking, due in part to the complexity of microbial biochemistry, but also to our inability to model and predict Hg biogeochemistry in terrestrial surface and subsurface systems. However, Hg cycling at the scale of an entire watershed or even large systems ultimately depends on the type of molecular-scale chemistry we have described here. What is required to extend to larger scales is a comprehensive computational catalog of thermodynamic quantities sufficient to describe Hg speciation in any given setting or environment. This data would then be used as input to mesoscale models, in which, typically, the gas, solution, and solid phases are assumed to be well-mixed continua in each representative volume, equilibrium chemical reactions are represented by mass action equations, kinetic reactions are described by ordinary differential equations, and transport is simulated by the advection–diffusion equation. Obtaining the data required for accurate continuum-scale modeling and assembling them in a multiscale simulation framework will be required to obtain predictive understanding of biotic and abiotic Hg transport and transformation in the environment.

In the environment, inorganic Hg is methylated by bacteria and archaea to form particularly toxic methylmercury, and we now know the proteins responsible for this process. We note that the Hg methylation conundrum was solved mainly by chemical reasoning, without the need for expensive computation. However, the details of the reaction and the complete biochemical pathway involved remain to be worked out. Much work is needed to arrive at a complete understanding of microbial uptake, intracellular transport and transformation, and export of Hg.

ACKNOWLEDGMENTS

We thank Anne Summers, Susan Miller, Liyuan Liang, Alex Johs, Demian Riccardi, Jing Zhou, Steve Tomanicek, Hao-Bo Guo, Tamar Barkay, Baohua Gu, Dwayne Elias,

Scott Brooks, Mircea Podar, Steve Brown, Richard Hurt Jr., Xiangping Yin, Romain Bridou, Steve Smith, and Judy Wall for fruitful collaborations over the past several years. This research was supported by the US Department of Energy (DOE), Office of Science, Office of Biological and Environmental Research, through the Mercury Scientific Focus Area at Oak Ridge National Laboratory (ORNL) and the Subsurface Biogeochemical Research (SBR) program at the University of Tennessee Knoxville and ORNL through Grant DE-SC0004895 from the US Department of Energy (DOE). ORNL is managed by UT-Battelle, LLC, for the US Department of Energy under contract DE-AC05-00OR22725.

REFERENCES

Afaneh, A. T., Schreckenbach, G., & Wang, F. Y. (2014). Theoretical study of the formation of mercury (Hg^{2+}) complexes in solution using an explicit solvation shell in implicit solvent calculations. *The Journal of Physical Chemistry B*, *118*(38), 11271–11283. http://dx.doi.org/10.1021/jp5045089.

Andrae, D., Haussermann, U., Dolg, M., Stoll, H., & Preuss, H. (1990). Energy-adjusted ab initio pseudopotentials for the 2nd and 3rd row transition elements. *Theoretica Chimica Acta*, *77*(2), 123–141. http://dx.doi.org/10.1007/Bf01114537.

Becke, A. D. (1993). Density-functional thermochemistry. 3. The role of exact exchange. *The Journal of Chemical Physics*, *98*(7), 5648–5652. http://dx.doi.org/10.1063/1.464913.

Bryantsev, V. S., Diallo, M. S., & Goddard, W. A. (2008). Calculation of solvation free energies of charged solutes using mixed cluster/continuum models. *The Journal of Physical Chemistry B*, *112*(32), 9709–9719. http://dx.doi.org/10.1021/jp802665d.

Chang, C. C., Lin, L. Y., Zou, X. W., Huang, C. C., & Chan, N. L. (2015). Structural basis of the mercury(II)-mediated conformational switching of the dual-function transcriptional regulator MerR. *Nucleic Acids Research*, *43*(15), 7612–7623. http://dx.doi.org/10.1093/nar/gkv681.

Cheesman, B. V., Arnold, A. P., & Rabenstein, D. L. (1988). Nuclear magnetic-resonance studies of the solution chemistry of metal-complexes. 25. Hg(thiol)3 complexes and Hg(Ii)-thiol ligand-exchange kinetics. *Journal of the American Chemical Society*, *110*(19), 6359–6364. http://dx.doi.org/10.1021/Ja00227a014.

Choi, S.-C., & Bartha, R. (1993). Cobalamin-mediated mercury methylation by *Desulfovibrio desulfuricans* LS. *Applied and Environmental Microbiology*, *59*, 290–295.

Choi, S.-C., Chase, T., Jr., & Bartha, R. (1994a). Enzymatic catalysis of mercury methylation by *Desulfovibrio desulfuricans* LS. *Applied and Environmental Microbiology*, *60*, 1342–1346.

Choi, S.-C., Chase, T., Jr., & Bartha, R. (1994b). Metabolic pathways leading to mercury methylation in *Desulfovibrio desulfuricans* LS. *Applied and Environmental Microbiology*, *60*, 4072–4077.

Colombo, M. J., Ha, J. Y., Reinfelder, J. R., Barkay, T., & Yee, N. (2013). Anaerobic oxidation of Hg(0) and methylmercury formation by *Desulfovibrio desulfuricans* ND132. *Geochimica et Cosmochimica Acta*, *112*, 166–177. http://dx.doi.org/10.1016/j.gca.2013.03.001.

Gregoire, D. S., & Poulain, A. J. (2016). A physiological role for Hg(II) during phototrophic growth. *Nature Geoscience*, *9*, 121–125. http://dx.doi.org/10.1038/ngeo2629.

Grimme, S., Antony, J., Ehrlich, S., & Krieg, H. (2010). A consistent and accurate ab initio parametrization of density functional dispersion correction (DFT-D) for the 94 elements H-Pu. *The Journal of Chemical Physics*, *132*, 154104.

Grimme, S., Ehrlich, S., & Goerigk, L. (2011). Effect of the damping function in dispersion corrected density functional theory. *Journal of Computational Chemistry*, *32*(7), 1456–1465. http://dx.doi.org/10.1002/jcc.21759.

Hong, L., Sharp, M. A., Poblete, S., Bieh, R., Zamponi, M., Szekely, N., … Smith, J. C. (2014). Structure and dynamics of a compact state of a multidomain protein, the mercuric ion reductase. *Biophysical Journal*, *107*(2), 393–400. http://dx.doi.org/10.1016/j.bpj.2014.06.013.

Johs, A., Harwood, I. M., Parks, J. M., Nauss, R. E., Smith, J. C., Liang, L. Y., & Miller, S. M. (2011). Structural characterization of intramolecular Hg (2+) transfer between flexibly linked domains of mercuric ion reductase. *Journal of Molecular Biology*, *413*(3), 639–656. http://dx.doi.org/10.1016/J.Jmb.2011.08.042.

Lafrance-Vanasse, J., Lefebvre, M., Di Lello, P., Sygusch, J., & Omichinski, J. G. (2009). Crystal structures of the organomercurial lyase MerB in its free and mercury-bound forms insights into the mechanism of methylmercury degradation. *The Journal of Biological Chemistry*, *284*(2), 938–944. http://dx.doi.org/10.1074/jbc.M807143200.

Lian, P., Guo, H. B., Riccardi, D., Dong, A. P., Parks, J. M., Xu, Q., … Guo, H. (2014). X-ray structure of a Hg^{2+} complex of mercuric reductase (MerA) and quantum mechanical/molecular mechanical study of Hg^{2+} transfer between the C-Terminal and buried catalytic site cysteine pairs. *Biochemistry*, *53*(46), 7211–7222. http://dx.doi.org/10.1021/bi500608u.

Marenich, A. V., Cramer, C. J., & Truhlar, D. G. (2009). Universal solvation model based on solute electron density and on a continuum model of the solvent defined by the bulk dielectric constant and atomic surface tensions. *The Journal of Physical Chemistry B*, *113*(18), 6378–6396. http://dx.doi.org/10.1021/jp810292n.

Parks, J. M., Guo, H., Momany, C., Liang, L. Y., Miller, S. M., Summers, A. O., & Smith, J. C. (2009). Mechanism of Hg–C protonolysis in the organomercurial lyase MerB. *Journal of the American Chemical Society*, *131*(37), 13278–13285. http://dx.doi.org/10.1021/Ja9016123.

Parks, J. M., Johs, A., Podar, M., Bridou, R., Hurt, R. A., Jr., Smith, S. D., … Liang, L. (2013). The genetic basis for bacterial mercury methylation. *Science*, *339*(6125), 1332–1335. http://dx.doi.org/10.1126/science.1230667.

Perdew, J. P., & Wang, Y. (1992). Accurate and simple analytic representation of the electron-gas correlation-energy. *Physical Review B*, *45*(23), 13244–13249. http://dx.doi.org/10.1103/Physrevb.45.13244.

Perdew, J. P., & Yue, W. (1986). Accurate and simple density functional for the electronic exchange energy: Generalized gradient approximation. *Physical Review B*, *33*(12), 8800–8802. http://dx.doi.org/10.1103/Physrevb.33.8800.

Peterson, K. A., & Puzzarini, C. (2005). Systematically convergent basis sets for transition metals. II. Pseudopotential-based correlation consistent basis sets for the group 11 (Cu, Ag, Au) and 12 (Zn, Cd, Hg) elements. *Theoretical Chemistry Accounts*, *114*(4–5), 283–296. http://dx.doi.org/10.1007/s00214-005-0681-9.

Pitts, K. E., & Summers, A. O. (2002). The roles of thiols in the bacterial organomercurial lyase (MerB). *Biochemistry*, *41*(32), 10287–10296. http://dx.doi.org/10.1021/bi0259148.

Ragsdale, S. W., & Pierce, E. (2008). Acetogenesis and the Wood-Ljungdahl pathway of CO_2 fixation. *Biochimica et Biophysica Acta*, *1784*(12), 1873–1898. http://dx.doi.org/10.1016/j.bbapap.2008.08.012.

Riccardi, D., Guo, H. B., Parks, J. M., Gu, B. H., Liang, L. Y., & Smith, J. C. (2013). Cluster-continuum calculations of hydration free energies of anions and group 12 divalent cations. *Journal of Chemical Theory and Computation*, *9*(1), 555–569. http://dx.doi.org/10.1021/Ct300296k.

Riccardi, D., Guo, H.-B., Parks, J. M., Gu, B., Summers, A. O., Miller, S. M., … Smith, J. C. (2013). Why mercury prefers soft ligands. *Journal of Physical Chemistry Letters*, *4*(14), 2317–2322. http://dx.doi.org/10.1021/jz401075b.

Schaefer, J. K., & Morel, F. M. M. (2009). High methylation rates of mercury bound to cysteine by Geobacter sulfurreducens. *Nature Geoscience*, *2*(2), 123–126. http://dx.doi.org/10.1038/NGEO412.

Schaefer, J. K., Rocks, S. S., Zheng, W., Liang, L. Y., Gu, B. H., & Morel, F. M. M. (2011). Active transport, substrate specificity, and methylation of Hg(II) in anaerobic bacteria. *Proceedings of the National Academy of Sciences of the United States of America*, *108*(21), 8714–8719. http://dx.doi.org/10.1073/pnas.1105781108.

Senn, H. M., & Thiel, W. (2009). QM/MM methods for biomolecular systems. *Angewandte Chemie (International Edition in English)*, *48*(7), 1198–1229. http://dx.doi.org/10.1002/anie.200802019.

Siegbahn, P. E. M., & Himo, F. (2011). The quantum chemical cluster approach for modeling enzyme reactions. *WIREs Computational Molecular Science*, *1*(3), 323–336. http://dx.doi.org/10.1002/wcms.13.

Smith, S. D., Bridou, R., Johs, A., Parks, J. M., Elias, D. A., Hurt, R. A., … Wall, J. D. (2015). Site-directed mutagenesis of HgcA and HgcB reveals amino acid residues important for mercury methylation. *Applied and Environmental Microbiology*, *81*(9), 3205–3217. http://dx.doi.org/10.1128/AEM.00217-15.

Stricks, W., & Kolthoff, I. M. (1953). Reactions between mercuric mercury and cysteine and glutathione. Apparent dissociation constants, heats and entropies of formation of various forms of mercuric mercapto-cysteine and mercapto-glutathione. *Journal of the American Chemical Society*, *75*(22), 5673–5681. http://dx.doi.org/10.1021/Ja01118a060.

Svetlitchnaia, T., Svetlitchnyi, V., Meyer, O., & Dobbek, H. (2006). Structural insights into methyltransfer reactions of a corrinoid iron-sulfur protein involved in acetyl-CoA synthesis. *Proceedings of the National Academy of Sciences of the United States of America*, *103*(39), 14331–14336. http://dx.doi.org/10.1073/Pnas.0601420103.

Warshel, A., & Levitt, M. (1976). Theoretical studies of enzymic reactions: Dielectric, electrostatic and steric stabilization of the carbonium ion in the reaction of lysozyme. *Journal of Molecular Biology*, *103*(2), 227–249.

Zhou, J., Riccardi, D., Beste, A., Smith, J. C., & Parks, J. M. (2014). Mercury methylation by HgcA: Theory supports carbanion transfer to Hg(II). *Inorganic Chemistry*, *53*(2), 772–777. http://dx.doi.org/10.1021/Ic401992y.